Ultrasound in Med. & Biol., Vol. 31, No. 8, pp. 1041–1049, 2005

0301-5629/05/$–see front matter

ELSEVIER

doi:10.1016/j.ultrasmedbio.2005.04.020

● *Original Contribution*

MONITORING STRUCTURAL CHANGES IN CELLS WITH HIGH-FREQUENCY ULTRASOUND SIGNAL STATISTICS

A. S. Tunis,*‡ G. J. Czarnota,†‡§ A. Giles‡ M. D. Sherar,*†‡‖ J. W. Hunt,*‡ and M. C. Kolios*§

Departments of *Medical Biophysics and †Radiation Oncology, University of Toronto, Toronto, ONT, Canada; ‡Ontario Cancer Institute/Princess Margaret Hospital, University Health Network, Toronto, ONT, Canada; §Department of Physics, Ryerson University, Toronto, ONT, Canada; and ‖London Regional Cancer Centre/London Health Sciences Centre and Department of Oncology, University of Western Ontario, London, ONT, Canada

(*Received* 8 *July* 2004, *revised* 4 *April* 2005, *in final form* 21 *April* 2005)

Abstract—We investigate the use of signal envelope statistics to monitor and quantify structural changes during cell death using an *in vitro* cell model. Using a f/2.35 transducer (center frequency 20 MHz), ultrasound backscatter data were obtained from pellets of acute myeloid leukemia cells treated with a DNA-intercolating chemotherapy drug, as well as from pellets formed with mixtures of treated and untreated cells. Simulations of signals from pellets of mixtures of cells were generated as a summation of point scatterers. The signal envelope statistics were examined by fitting the Rayleigh and generalized gamma distributions. The fit parameters of the generalized gamma distribution showed sensitivity to structural changes in the cells. The scale parameter showed a 200% increase ($p < 0.05$) between untreated and cells treated for 24 h. The shape parameter showed a 50% increase ($p < 0.05$) over 24 h. Experimental results showed reasonable agreement with simulations. The results indicate that high-frequency ultrasound signal statistics can be used to monitor structural changes within a very low percentage of treated cells in a population, raising the possibility of using this technique *in vivo*. (E-mail: mkolios@ryerson.ca)

Key Words: **Tissue characterization, High-frequency ultrasound, Envelope statistics, Generalized gamma, Rayleigh, Treatment monitoring, Cell/nucleus structure, Ultrasonics, Acute myeloid leukemia, Computer simulation.**

INTRODUCTION

It has previously been shown that high-frequency ultrasound (HFUS) is sensitive to the structural changes that occur in acute myeloid leukemia (AML) cells during apoptosis, a form of programmed cell death. These structural changes, including nuclear condensation, nuclear fragmentation and other changes, produce a marked increase in the integrated backscatter (IB) signal amplitude and changes in the frequency-dependence of the power spectra (Kolios et al. 2002, 2003; Czarnota et al. 1997, 1999, 2002). It has been possible to differentiate noninvasively between dying and viable cell populations *in vitro* and *in vivo* based on these changes in IB. Although the limited penetration depth of HFUS restricts its use to superficial sites, this technology could prove valuable for the evaluation of the response to therapy of superficial tumors, allowing for an early determination of the treatment efficacy. This rapid assessment of treatment response could potentially allow for therapy modification to treat the disease better, sparing the patient population from unnecessary comorbidity.

Making the distinction between viable and dying cells *in vivo* is more difficult than *in vitro* because the changes that occur in cell and tissue structure can affect the IB in multiple ways. As an alternative technique for monitoring cell death *in vivo*, we have investigated the statistics of the envelope of HFUS backscatter signals for information related to changes in cellular structure. Changes to the scatterer cross-section and spatial arrangement are predicted to affect the statistics of the signal envelope. The technique of envelope statistics analysis has been applied experimentally to tissue classification using lower-frequency ultrasound (US). Shankar et al. (1993, 1996, 2001, 2003) and Molthen et al. (1995, 1998) demonstrated its use for differentiating masses in breast tissue and Hao et al. (2001a, 2001b,

Address correspondence to: Dr. M. C. Kolios, Department of Physics, Ryerson University, 350 Victoria Street, Toronto, Ontario M5B 2K3 Canada. E-mail: mkolios@ryerson.ca

2002) demonstrated its use for differentiating between infarcted and viable tissue in the heart. Recently, and at higher frequencies, it has also been applied to tissue classification of skin by Raju and Srinivasan (2002) and Raju et al. (2003). In this work, we have applied this technique to the task of monitoring pellets of AML cells treated for different times with cisplatin. To determine the sensitivity of this technique, we examined pellets formed with mixtures of treated and untreated AML cells. The pellets are formed by centrifuging cells to form a compacted aggregate of cells. The cells are packed closely together, emulating the cell packing in tissues. The HFUS backscatter from cell pellets is, therefore, similar to that from cancer tissues.

Theory

A HFUS backscatter signal is composed of contributions from many individual scatterers. Each scatterer contributes an amplitude and a phase to the received signal. This can be modeled by eqn (1) (Raju and Srinivasan 2002):

$$re^{j\Psi} = \sum_{i=1}^{n} r_i e^{j\theta i}. \tag{1}$$

The amplitude and the phase (r_i and θ_i) contribution from each scatterer is determined by its position, size and acoustic properties. Because there is a statistical distribution of these properties, the amplitude and phase (r and ψ) of the received signal will also have a probability distribution.

Numerous probability density functions (PDFs) have been proposed to describe the statistics of ultrasonic backscatter (Dutt and Greenleaf 1994; Narayanan et al. 1994; Shankar et al. 1996; Raju and Srinivasan 2002). We investigated the use of two of these distributions, the Rayleigh distribution (Strutt 1880) and the generalized gamma (GG) distribution (Stacy 1962).

The Rayleigh distribution was chosen because it is often used as a basic model of the statistics of US backscatter. The GG distribution was chosen because recent work by Raju and Srinivasan (2002) has shown it to provide a good fit to experimental HFUS backscatter data and, in our initial investigations (Tunis 2005; Tunis et al. 2005), it showed good sensitivity to the changes that occur in cell death.

The Rayleigh PDF, often used as a simplified description of the statistics, is based on three assumptions. First, the scatterers are much smaller than the wavelength. Second, the resolution cell of the US system, in this case of lateral dimension 250 μm and axial 140 μm, contains a large number of scatterers. Finally, the scatterers are located randomly in the medium. Because we are dealing with pellets of cells, where the cells are compacted side-by-side, it can be speculated that the major acoustic interface is the cytoplasm nucleus boundary. Experimental evidence suggests that, at high frequencies, the nucleus is the primary scatterer (Czarnota 2002; Beaulieu et al. 2002).

In the AML cells used, the nucleus was approximately 9 μm in diameter, smaller than the wavelength range of 50 to 150 μm. Furthermore, if one assumes that there is one scatterer per cell, then there are approximately 4600 scatterers per resolution volume. However, there is some inherent degree of organization of the cells within a pellet, making it not a completely random medium. The Rayleigh PDF is given in eqn (2).

$$p(r) = \frac{r}{\sigma^2} e^{\frac{-r^2}{2\sigma^2}} \tag{2a}$$

$$r \geq 0; \quad \sigma > 0 \tag{2b}$$

where the probability, p, of a Rayleigh-distributed signal having an amplitude r is a function of the scale parameter, σ, which represents a measure of the mean signal amplitude.

The GG PDF was first proposed by Stacy (1962). Its application to modeling US signals was proposed independently by Raju and Srinivasan (2002) and Shankar (2001). The GG PDF is given in eqn (3).

$$p(r) = \frac{c r^{c\upsilon - 1}}{a^{c\upsilon}\Gamma(\upsilon)} e^{-(\frac{r}{a})^c} \tag{3a}$$

$$r \geq 0; a \geq 0; \upsilon \geq 0; c \geq 0 \tag{3b}$$

where $\Gamma(\upsilon)$ is the incomplete gamma function, a is the scale parameter, which is related to the mean of the PDF, and c and υ are two shape parameters, representing the positions of the left and right tails of the PDF, respectively.

The GG PDF is equivalent to a number of other PDFs as special cases, including the Rayleigh when $c = 2$ and $\upsilon = 1$. The GG PDF is very similar to the generalized Nakagami PDF proposed by Shankar (2001) to model US statistics. In the context of the generalized Nakagami PDF, Shankar has proposed that the scale parameter (a) is a measure of average backscattered power and can be related to the average scatterer cross-section (Shankar 2001b). As described by Hunt et al. (2002), the average backscattered power is dependent on both the geometrical cross-section and scatterer organization and, therefore, the a parameter reflects both. Based on the interpretation proposed by Shankar (2001), the shape parameters of the GG PDF (c and υ) relate to the scatterer number density. The ratio of the two parameters, c/υ, can be used as an estimate of effective scatterer number density.

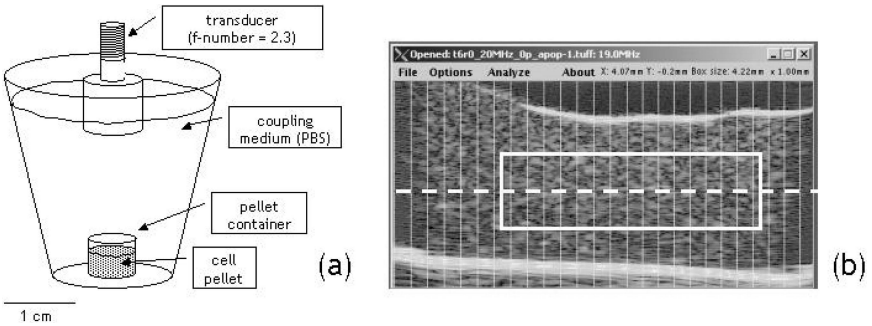

Fig. 1. (a) Schematic showing positioning of the transducer over the cell pellet. The transducer was scanned linearly across the pellet to acquire images and RF data from slices through the pellet. (b) The JAVA program allows for selection of a homogeneous ROI within saved data. The box (4.22 × 1 mm) shows selected region; (——) the transducer focus; (vertical lines) positions where RF lines were acquired.

Recent experimental evidence indicates that, in the *in vitro* model of cells in suspension at low volumetric concentrations, with this interpretation of the parameters the GG PDF does apply to a biologic model (Tunis 2005). However, it remains speculative as to whether this interpretation holds for high concentrations of cells or cell pellets.

METHODS

Cell preparation

AML cells were cultured at a density of 3×10^5 cells/mL in α minimum essential medium (GIBCO 11900, Rockville, MD, USA) supplemented with 5% fetal bovine serum (Cansera International, Etobicoke, ON, Canada) at 37 °C. Cells were treated for 0, 3, 6, 9, 12, 18, 24 and 48 h with 10 μg/mL of cisplatin in the timed exposure experiment. The cells were then spun in a swinging bucket centrifuge for 10 min at 2000 *g*, to form pellets. The pellets are a compacted aggregate of cells, emulating the cell packing in tissues. HFUS data and images were acquired within 10 min of pellet formation.

To investigate the sensitivity of the signal statistics to changes in a small percentage of a cell population, pellets of mixed populations of cells were prepared. In the first experiment, the cells treated for 24 h showed pyknotic nuclei and a maximum increase in IB of $\approx$ 13 dB was seen at approximately 24 h (Figs. 3 and 5). We similarly prepared the AML cells and treated some for 24 h with 10 μg/mL of cisplatin. This time, the treated cells were mixed with untreated cells to form mixtures containing 0%, 2.5%, 5%, 10%, 20%, 40%, 60%, 80% and 100% treated cells. The mixtures were then spun in a swinging bucket centrifuge for 10 min at 2000 *g* to form pellets and HFUS data and images were acquired within 10 min of pellet formation. It should be noted that not all the treated cells respond to the treatment; therefore, the percentages represent an upper bound to the concentration of treated cells.

After the HFUS data acquisition, the pellets were fixed in 10% formalin solution (Fisher Scientific, Nepean, ON, Canada) for a minimum of 2 days. The fixed pellet of cells was carefully removed from the pellet holder and placed in a dish of agar gel, to preserve the shape of the pellet. The pellet was sectioned and placed in a cassette for paraffin embedding, so that the microtome sections were taken from the same plane as the HFUS images. The sections were stained with hematoxylin and eosin (H&E) to examine cell packing in the pellet and morphology changes in the cells. Visual inspection of the histology of the pellets of mixtures indicated a uniform distribution of treated and untreated cells in the pellet. Both experiments were repeated to test for reproducibility, the time-course 4 times and the mixture twice.

Data acquisition

Data were acquired using a commercial HFUS scanner (VS-40B, VisualSonics Inc., Toronto, ON, Canada) with a focused transducer manufactured by VisualSonics (f-number 2.35, focal length 20 mm, center frequency 20 MHz, band width 100%). The pellet container was affixed to the bottom of a plastic dish using vacuum grease and phosphate-buffered saline (PBS) was used as a coupling medium to the transducer (Fig. 1). B-scan images and radiofrequency (RF) data (A-scans) were recorded from independent locations separated by at least one beam width (250 μm) within the pellet. The B-scan images were recorded in real time and the RF data were acquired over a period of approximately 2 to 3 min. To minimize any motion of the pellet induced by the transducer oscillation, the transducer was located a significant distance from the pellet (approximately 1.5 to 2 cm) during the imaging. Also, when recording B-scan images, images were recorded during both forward and reverse sweeps of the transducer. During this process,

no noticeable motion was detected between forward and reverse frames, indicating that there was minimal motion of the cell pellet. Using custom software written in JAVA (JDK 1.4.1, Sun Microsystems, Inc., Santa Clara, CA, USA), RF data were extracted from a relatively homogeneous region-of-interest (ROI) within the stored data. The focus of the transducer was positioned 1.5 mm below the surface of the pellet. The ROI was selected to be from 0.5 mm above the focus to 0.5 mm below the focus (Fig. 1). This is well within the depth of field (3.12 mm), so that the decrease in signal over the 1-mm ROI would be primarily because of attenuation. To correct for this, the attenuation in dB/mm was determined as the decrease in mean signal envelope over the 1-mm depth. Using this attenuation value, the data were corrected for attenuation by applying depth-dependent amplification. The envelope statistics were analyzed both with and without the attenuation correction, yielding the same trends (data not shown).

Simulations

Simulated RF data sets were generated to model the scattering of HFUS from cells *in vitro* using the method of Hunt et al. (1995, 2002). The model simulated the backscatter signals for a pellet of cells, assuming that the signals are formed only from cellular nuclei (Czarnota et al. 2002; Hunt et al. 2002). A range of scatterers was explored in these basic simulations, but all assumed that similar scattering occurs during the treatment of each cell. The simplified model is presented in Fig. 2, for 16 point scatterers in a slightly random distribution. As the cell is treated, the nucleus goes through a series of structural changes, as shown in Fig. 2. This is modeled as a reduction in the size of the nucleus. The primary effect of this process is an increase in the randomization of the locations of the scatterers, leading to a general increase in backscattered signal (Hunt et al. 2002).

The simulation was performed in two dimensions, with the actual system and transducer properties being incorporated into the modeling of the received signal. The simulated signal was scaled by a constant value to make the IB of an untreated pellet the same for the simulated and the experimental data. For the current study, the pellets were modeled as a mixture of untreated cells with treated cells. Based on the observed histology (Figs. 3 and 7), the treated cells were modeled as having a nuclear diameter equal to 40% of the cell's diameter, while untreated cells were modeled with a nuclear diameter equal to 90% of the cell's diameter. Simulations were performed corresponding to the range of proportions of treated and untreated cells used in the experiments.

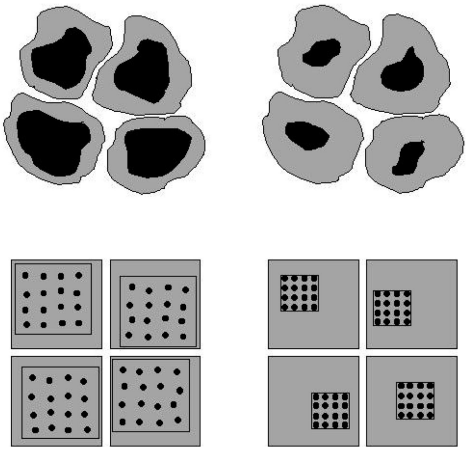

Fig. 2. Schematic of cells treated with cisplatin, showing (top row) reduced size of the nucleus. As the cell dies, the nuclear volume (black) condenses. This results in an increase in randomization of positions of the nucleus within the cytoplasm (grey). The model of Hunt et al. (2002) was used for the simulation. (bottom row) The nucleus is modeled in 2-D as a set of 16 point scatterers constrained to a region defined as the nucleus.

Data analysis

Based on the RF data selected from the ROI, PDF fit parameters were determined using an implementation of the maximal likelihood estimation (MLE) routine (Matlab 6.1, The MathWorks Inc., Natick, MA, USA). The MLE routine maximizes the log-likelihood function of the distribution for the given data set.

The goodness of fit of the two distributions was evaluated by the Kolmogorov–Smirnov (KS) goodness-of-fit test (Patel et al. 1976; Stephens 1970). This test is based on the maximum deviation between the theoretical cumulative density function (CDF) and the empirical CDF. The KS value can be used to assess the validity of the assumptions made in the Rayleigh distribution for the data in question.

As a measure of the signal amplitude, the midband fit of the normalized power spectrum was calculated (Lizzi et al. 1983, 1997; Kolios et al. 2002). The average power spectrum was determined by calculating the Fourier transform of each RF line within the ROI, then averaging the spectra of multiple lines. The average power spectrum was then divided by the spectrum of a reflection off a quartz flat, to remove system effects and to determine the normalized power spectrum. A straight line was fit to the normalized power spectrum using linear regression analysis and the midband fit was determined as the value (dBr) of the line at the center frequency of the transducer.

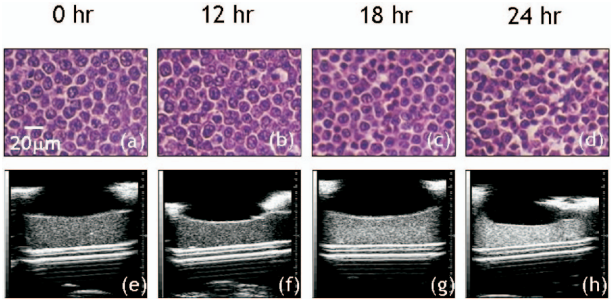

Fig. 3. (a)–(d) Light microscopy (40 × magnification) of H&E-stained sections of pellets of AML cells treated for 0, 12, 18 and 24 h with cisplatin. (e)–(h) B-scan images of the same pellets with a 20-MHz f/2.35 transducer. FOV is 8 mm by 8 mm; pellet = speckled region in center, hyperechoic line across the bottom is the plastic pellet container; sides of the pellet container are visible in top corners. The pellet shows a marked increase in intensity as it is treated longer.

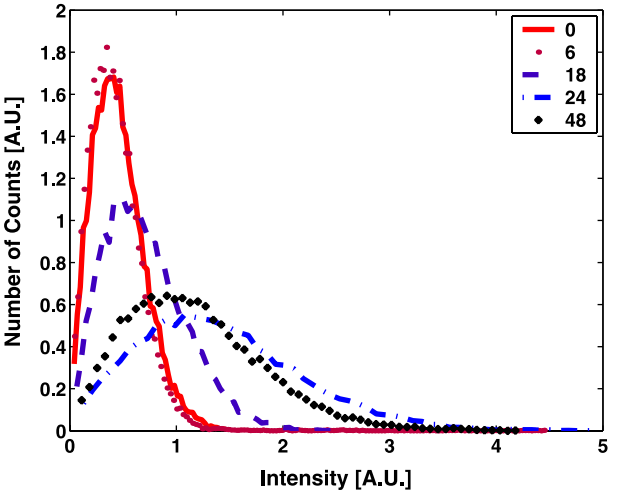

Fig. 4. Histograms of amplitude of the envelope of HFUS data acquired from pellets of AML cells treated for 0, 6, 18, 24 and 48 h with cisplatin. Histograms are normalized to an area of one to allow comparison between histograms. The dramatic change in scale corresponds to an increase in backscatter intensity. There are also more subtle changes to the shapes of the histograms as cells are treated longer, as indicated by changes in the c/v parameter.

RESULTS

Time exposure

As the cells were exposed to cisplatin, a series of changes to the structure of the cell and its nucleus were observed (Fig. 3). These included condensation of the nuclei, stained dark in Fig. 3, a classic sign of several forms of cell death. At the early time points where there were no visible changes in histology, no changes were apparent in the HFUS signal. When cells were treated for longer periods of time, there were visible changes in histology and a marked increase in the backscattered intensity, with a maximum increase of approximately 13 dB between the untreated sample and the sample treated for 24 h. The marked increase in IB is also apparent in the change in the scale of the histograms of HFUS data (Fig. 4). At all exposure times, the Rayleigh and GG distribution both provided reasonable fits to the data, as determined by the KS goodness-of-fit parameter. Although not statistically significant, the GG distribution provided a better fit, with KS values being approximately half the Rayleigh distribution KS values. No significant trends were observed with increased exposure time (Table 1).

The GG a parameter increased consistently for the samples treated from 0 through 24 h, for all the experiments performed (Fig. 5). The GG c/v parameter shows large variability between the four experiments in the values for samples treated for a short time, up to 12 h, although all the experiments show an increase over the period from 12 to 24 h (Fig. 6). The increases in both a and c/v between 0 and 24 h were significant ($p < 0.05$). This increase in c/v may be interpreted as an increase in number density between 12 and 24 h, based on an interpretation proposed by Shankar (2001). The treated cells are slightly smaller, which may contribute to an increase in scatterer number density.

Mixture of treated and untreated cells

To evaluate the sensitivity of the HFUS signal statistics to a low percentage of treated cells within a pellet, pellets containing a mixture of treated and untreated cells were prepared. As previously, the most striking visual change was the condensation of the nucleus, clearly visible in the H&E-stained sections of pellets (Fig. 7). The histology also demonstrates that the treated cells are mixed uniformly throughout the pellets.

The corresponding B-scan images show an increase in the backscatter intensity for pellets containing a higher concentration of treated cells. Despite logarithmic compression, an increase in brightness is visible between the B-scans of pellets formed with 0% and 2.5% treated cells

Table 1. KS goodness-of-fit parameter for the Rayleigh and generalized gamma distribution fits to data from untreated AML cells and AML cells exposed to cisplatin for 24 h

Treatment time (h)	Rayleigh	GG
0	0.02 ± 0.01	0.011 ± 0.004
24	0.014 ± 0.01	0.006 ± 0.004

Values represent the mean of four experiments, with SDs between the experiments. Although there is a slight increase in the goodness-of-fit from 0 to 24 h (decrease of the KS values), the changes are not significant.

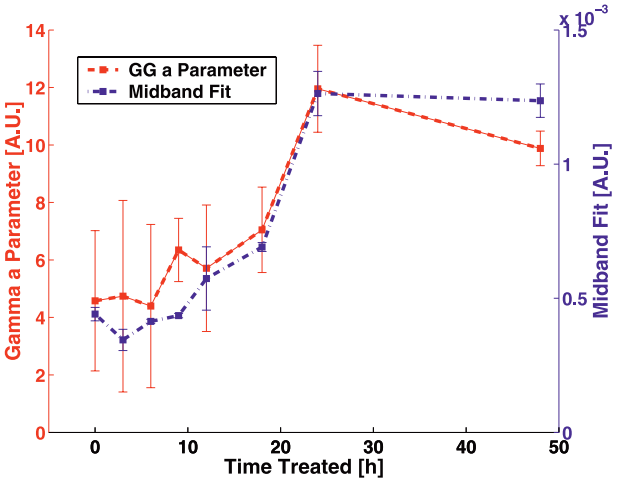

Fig. 5. The GG *a* parameter with 95% confidence intervals (left hand axis) along with midband fit and SDs (right hand axis) for HFUS data from cells treated with cisplatin. Values are the mean of four experiments at 0, 3, 6, 12 and 24 h of exposure and the mean of two experiments at 9 and 48 h of exposure.

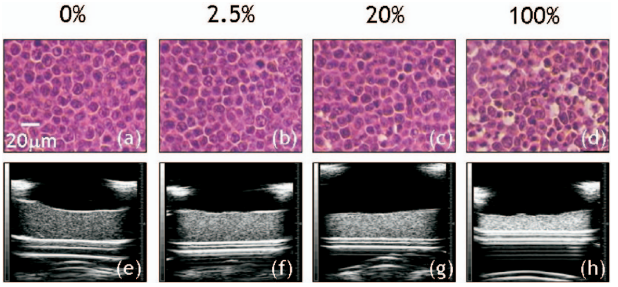

Fig. 7. (a)–(d) Light microscopy (40 × magnification) of H&E-stained sections of pellets formed with mixtures of untreated and (a) 0%, (b) 2.5%, (c) 20% and (d) 100% cisplatin-treated AML cells (24 h exposure). (e)–(h) B-scan images of the same pellets with a 20-MHz f/2.35 transducer. The FOV is 8 mm by 8 mm, pellet is speckled region in center, hyperechoic line across bottom is the bottom of the plastic pellet container; sides of pellet container are visible in top corners. There is a significant increase in intensity as the percentage of treated cells is increased, even between the pellets formed with 0% and 2.5% treated cells.

(Fig. 7), corresponding to a 3-dB increase in the midband fit. As the percentage of treated cells in the pellet increased, the signal intensity increased, producing large changes in the shape of the histogram of signal amplitude (Fig. 8). Based on the KS goodness of fit, the Rayleigh and GG distributions both provided reasonable fits to the empirical and simulated data for all mixtures of treated and untreated cells. Again, the GG provided a better fit and there were no significant trends in the KS values with mixture composition (data not shown).

The GG scale parameter (*a*) increased as the percentage of treated cells increased, corresponding to an increase in the midband fit of approximately 12 dB (Fig. 9). The GG *a* parameter for the simulated data shows a similar trend. The shape parameter (c/υ) shows a generally increasing trend, as the percentage of treated cells increases (Fig. 10). The increases in both *a* and c/υ

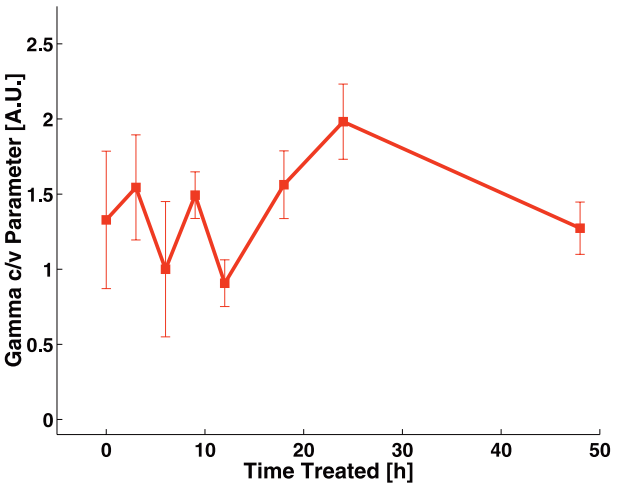

Fig. 6. The GG c/υ parameter with 95% confidence intervals for HFUS data from pellets of cells treated for 0 to 48 h with cisplatin. Values are the mean of four experiments at 0, 3, 6, 12 and 24 h of exposure and the mean of two experiments at 9 and 48 h of exposure. There is large variability at early time-points between the four experiments, with a consistent increase between 12 and 24 h.

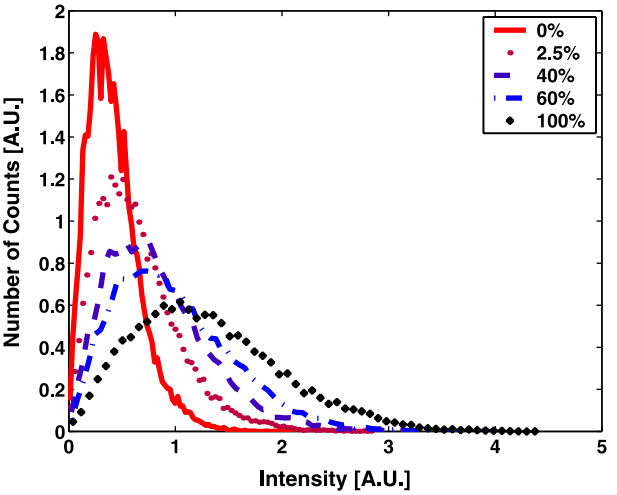

Fig. 8. Histograms of the amplitude of the envelope of HFUS data acquired from pellets of cells formed with varying mixtures of AML cells treated with cisplatin. Histograms are normalized to an area of one to allow comparison between histograms. The dramatic change in scale corresponds to an increase in IB; there are also more subtle changes to the shapes of the histograms as the concentration of treated cells increases.

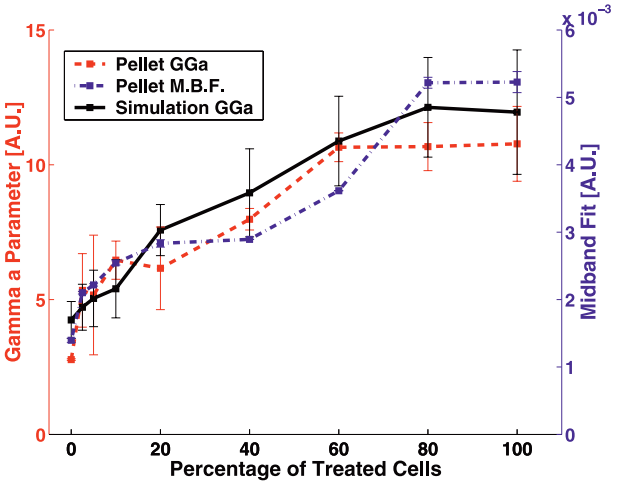

Fig. 9. The GG *a* parameter, with 95% confidence intervals (left hand axis) along with midband fit and SDs (right hand axis) for HFUS data from cell pellets and simulations. Values are the mean of two experiments at all concentrations except 40% and 60%, where there was only one experiment. There is reasonable agreement between cell pellet data and simulated data, with similar increases as the concentration increases from 0% to 100%.

between pellets containing 0% and 100% treated cells were significant ($p < 0.05$). Although the GG a parameter is sensitive to the scaling applied to the simulated data to make the amplitude of the simulated signal equal to the amplitude of signals from the experiments, the GG c/υ parameter is independent of this scale factor. There is reasonable agreement between the shape parameters of the experimental data and the simulated data, with both showing similar values.

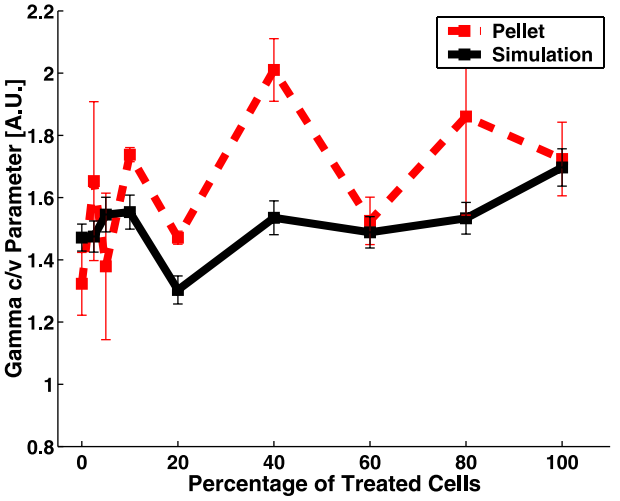

Fig. 10. The GG c/υ parameter, with 95% confidence intervals for HFUS data from cell pellets and simulations. Values are the mean of two experiments at all concentrations except 40% and 60%, where there is only one experiment. There is general agreement between cell pellet data and simulated data.

DISCUSSION

High-frequency US data were collected from pellets of AML cells treated for different times with cisplatin. To assess the lower limit of detection of cell death, HFUS data were also collected from pellets containing mixtures of treated and untreated AML cells. The pellets provide a reasonable model for HFUS backscatter from solid tumors. Results from current investigations indicate that the backscattered power spectra and envelope statistics of pellets of non-Hodgkin's lymphoma cells and the implanted non-Hodgkin's lymphoma tumors are similar. Simulated data were generated to model the data acquired from pellets containing a mixture of cells, based on the assumption that the cell nucleus is the primary scatterer, as indicated by recent experimental evidence (Czarnota 2002; Beaulieu et al. 2002).

Signal envelope statistics of the data were analyzed by fitting the Rayleigh and GG PDFs using the MLE parameter estimation technique. Based on the KS goodness-of-fit test, both PDFs provide fairly good fits to the cell pellet data. Although the difference between the goodness of fit of the two distributions was not statistically significant, the GG distribution provided a consistently better fit than did the Rayleigh distribution. This was true for both the experimental and simulated data. This leads to a question of whether or not the assumptions made to derive the Rayleigh distribution are valid. Because the cell size is smaller than the wavelength (15 μm vs. 75 μm) and because there are approximately 4600 cells per resolution volume, the least convincing of the assumptions is the requirement that the scatterers be at random locations. As can be seen in the histology, the organization of the cells in the pellet could be described as being a set of spheres packed together. Because the cells are not identical spheres, the pellet is not a perfect lattice but there is, nonetheless, some degree of order in the pellet. This regular spacing within the pellet may result in the Rayleigh distribution providing a poor description of the true statistics. Surprisingly, however, there was no statistically significant trend in the goodness of fit of the Rayleigh distribution for either the timed exposure or for the mixtures of treated and untreated cells. One might expect an increased goodness of fit for the pellets formed with treated cells, caused by increased apparent randomization.

The GG *a* parameter was greater for cells treated for a longer time with cisplatin. The ratio of the shape parameters (c/υ) of the GG distribution also shows a consistent increase from 12 to 24 h. The *a* parameter of the GG distribution was greater for pellets with a higher

concentration of treated cells. The ratio of the shape parameters (c/υ) of the GG distribution showed a slight increase with higher concentrations of treated cells. There was reasonable agreement between the parameters for the cell data and the simulated data.

It has been proposed that the ratio c/υ can be related to effective scatterer number density, based on simulations and work in phantoms (Shankar 2001) and experiments with solutions of low volumetric concentrations of cells *in vitro* (Tunis 2005). However, it remains unclear as to what could cause an increase in effective number density in AML cells treated with cisplatin. As stated previously, the majority of our experimental evidence points to the nucleus as the primary scattering source in pellets (Czarnota 2002; Beaulieu et al. 2002). Although the structure of the nucleus does change dramatically during treatment with cisplatin, the spacing between nuclei and, hence, the number density seem to remain fairly constant, as evidenced by the histology. A similar increase was seen in c/υ with the simulated data, where number density is definitely constant; the only change is the increased randomization of treated cells compared with untreated. This implies that, perhaps, the randomization of the scatterers affects the effective number density as determined by the ratio of the GG parameters c/υ.

All three GG fit parameters showed large changes for pellets formed with between 0% and 20% treated cells. A very large increase was observed in the a parameter between 0% and 2.5%, with continual increases up to 20%, and the ratio c/υ showed large fluctuations over the range from 0% to 20%. The similar trends observed in the simulated data over this range, again, imply that randomization is important in determining the nature of backscattered US; however, the discrepancies do illustrate that there are complexities that must be addressed in the model. Although we do not fully understand the cause of the sensitivity to changes in a small percentage of cells, these results are promising, because, clinically, there may be a very low percentage of cells responding to treatment at any one time. It is, thus, necessary to be able to detect changes within a small percentage of a population of cells.

We are currently performing experiments further to investigate the effects of randomization and number density on the envelope statistics. Suspensions of cells provide a system with increased randomization compared with a pellet system. HFUS backscatter signals from suspensions and pellets of cells of varying sizes indicate that number density and randomization both affect the statistics. The results indicate that, as predicted by Shankar (2001), the ratio c/υ is related to number density for dilute suspensions of cells, irrespective of cell diameter (Tunis 2005). We are also investigating the application of this technique *in vivo* using two animal models, mouse mammary tissue during the involution process and the response of implanted non-Hodgkin's lymphoma tumors to chemotherapy treatment. Results from the animal experiments as well as preliminary results from a clinical trial, where we have collected HFUS data from superficial tumors during treatment, indicate that HFUS can be used to monitor structural changes in cells *in vivo* (Tunis et al. 2004; Tunis 2005).

CONCLUSIONS

Previous work has demonstrated that signal statistics of backscattered US can be used for tissue characterization. It has been shown that the statistics are affected by macroscopic differences in tissue structure, such as between benign and malignant breast tumors (Shankar et al. 2001, 2003) or between skin tissue from different regions (Raju and Srinivasan 2002). It has also been shown that, in phantoms (Shankar 2001; Dutt and Greenleaf 1994), there is a relationship between the statistics and the scattering interaction. Our previous work has shown that the changes that occur during cell death affect the backscattered US intensity and frequency content (Kolios et al. 2002, 2003; Czarnota et al. 1999, 2002). The results of this investigation demonstrate that HFUS signal statistics are also affected by the changes at a subcellular level that occur during cell death.

The shape parameters of the GG distribution are sensitive to structural changes within cells. The agreement between the simulated and experimental data suggests that the randomization of the positions of scatterers is an important factor in determining the shape parameters of the GG distribution. The GG fit parameters were also shown to be sensitive to a small percentage of treated cells within a pellet. Changes in the parameters, as well as the midband fit, were observed between pellets of untreated cells and pellets containing 2.5% treated cells. This demonstrates that this technique could be applicable in a clinical setting, where it would be necessary to detect changes that may occur in a small percentage of the cells in the tissue.

The changes observed in the HFUS signal statistics provide further insight as to how the structural changes that occur during cell death affect backscattered HFUS signals. This technique shows promise for its ability to monitor structural changes in populations of cells during cell death.

Acknowledgements—The authors would like to acknowledge Arthur Worthington and Linda Taggart for technical support. The VisualSonics ultrasound instrument was purchased with the financial support of the Canada Foundation for Innovation, the Ontario Innovation Trust and Ryerson University. This work was supported by the Whitaker

Foundation (#RG-01-0141) and the Canadian Institutes of Health Research (#15353).

REFERENCES

Beaulieu J, Vlad R, Taggart L, et al. High-frequency ultrasound characterization of microcellular components. In: Proceedings of the 10th Congress of the World Federation for Ultrasound in Medicine and Biology, 2002, Montreal, Canada.

Czarnota GJ. Ultrasound imaging of apoptosis in vivo: Effects of subcellular nuclear morphology and cell membrane morphology. In: Proceedings of the 10th Congress of the World Federation for Ultrasound in Medicine and Biology, 2002, Montreal, Canada.

Czarnota GJ, Kolios MC, Abraham J, et al. Ultrasound imaging of apoptosis: High-resolution non-invasive monitoring of programmed cell death in vitro, in situ and in vivo. Br J Cancer 1999;81(3):520–527.

Czarnota GJ, Kolios MC, Hunt JW, Sherar MD. Ultrasound imaging of apoptosis DNA-damage effects visualized. Methods Mol Biol 2002;203:257–277.

Czarnota GJ, Kolios MC, Vaziri H, et al. Ultrasonic biomicroscopy of viable, dead and apoptotic cells. Ultrasound Med Biol 1997;23(6): 961–965.

Dutt V, Greenleaf JF. Ultrasound echo envelope analysis using a homodyned K distribution signal model. Ultrason Imaging 1994; 16(4):265–287.

Hao X, Bruce CJ, Pislaru C, Greenleaf JF. Identification of reperfused infarcted myocardium from high frequency intracardiac ultrasound images using homodyned K distribution. IEEE Ultrason Sympos 2001a;1189–1192.

Hao X, Bruce CJ, Pislaru C, Greenleaf JF. Segmenting high frequency intracardiac ultrasound images of myocardium into infarcted, ischemic, and normal regions. IEEE Trans Med Imaging 2001b;20(12): 1373–1383.

Hao X, Bruce CJ, Pislaru C, Greenleaf JF. Characterization of reperfused infarcted myocardium from high-frequency intracardiac ultrasound imaging using homodyned K distribution. IEEE Trans Ultrason Ferroelec Freq Control 2002;49(11):1530–1542.

Hunt JW, Worthington AE, Kerr AT. The subtleties of ultrasound images of an ensemble of cells: Simulation from regular and more random distributions of scatterers. Ultrasound Med Biol 1995; 21(3):329–341.

Hunt JW, Worthington AE, Xuan A, et al. A model based upon pseudo regular spacing of cells combined with the randomisation of the nuclei can explain the significant changes in high-frequency ultrasound signals during apoptosis. Ultrasound Med Biol 2002;28(2): 217–226.

Kolios MC, Czarnota GJ, Lee M, Hunt JW, Sherar MD. Ultrasonic spectral parameter characterization of apoptosis. Ultrasound Med Biol 2002;28(5):589–597.

Kolios MC, Taggart L, Baddour RE, et al. An investigation of backscatter power spectra from cells, cell pellets and microspheres. In: Proceedings of the 2003 IEEE International Ultrasonics Symposium 2003;752–757.

Lizzi FL, Astor M, Feleppa EJ, Shao M, Kalisz A. Statistical frame work for ultrasonic spectral parameter imaging. Ultrasound Med Biol 1997;23(9):1371–1382.

Lizzi FL, Greenebaum M, Feleppa EJ, Elbaum M. Theoretical framework for spectrum analysis in ultrasonic tissue characterization. J Acoust Soc Am 1983;73(4):1366–1373.

Molthen RC, Shankar PM, Reid JM. Characterization of ultrasonic B-scans using non-Rayleigh statistics. Ultrasound Med Biol 1995; 21(2):161–170.

Molthen RC, Shankar PM, Reid JM, et al. Comparisons of the Rayleigh and K-distribution models using *in vivo* breast and liver tissue. Ultrasound Med Biol 1998;24(1):93–100.

Narayanan VM, Shankar PM, Reid JM. Non-Rayleigh statistics of ultrasonic backscattered signals. IEEE Trans Ultrason Ferroelec Freq Control 1994;41(6):845–852.

Patel JK, Kapadia CH, Owen DB. Handbook of statistical distributions. Statistics, textbooks and monographs. Vol. 20. New York: M. Dekker, 1976.

Raju BI, Srinivasan MA. Statistics of envelope of high-frequency ultrasonic backscatter from human skin in vivo. IEEE Trans Ultrason Ferroelec Freq Control 2002;49(7):871–882.

Raju BI, Swindells KJ, Gonzalez S, Srinivasan MA. Quantitative ultrasonic methods for characterization of skin lesions *in vivo*. Ultrasound Med Biol 2003;29(6):825–838.

Shankar PM. Ultrasonic tissue characterization using a generalized Nakagami model. IEEE Trans Ultrason Ferroelec Freq Control 2001;48(6):1716–1720.

Shankar PM, Dumane VA, George T, et al. Classification of breast masses in ultrasonic B scans using Nakagami and K distributions. Phys Med Biol 2003;48(14):2229–2240.

Shankar PM, Dumane VA, Reid JM, et al. Classification of ultrasonic B-mode images of breast masses using Nakagami distribution. IEEE Trans Ultrason Ferroelec Freq Control 2001;48(2):569–580.

Shankar PM, Molthen R, Narayanan VM, et al. Studies on the use of nonRayleigh statistics for ultrasonic tissue characterization. Ultrasound Med Biol 1996;22(7):873–882.

Shankar PM, Reid JM, Ortega H, Piccoli CW, Goldberg BB. Use of non-Rayleigh statistics for the identification of tumors in ultrasonic B-scans of the breast. IEEE Trans Med Imaging 1993;12(4):687–692.

Stacy EW. A generalization of the gamma distribution. Ann Math Stats 1962;33(3):1187–1192.

Stephens MA. Use of the Kolmogorov–Smirnov, Cramer–Von Mises and related statistics without extensive tables. J Roy Stat Soc Ser B Method 1970;32(1):115–122.

Strutt JW. On the resultant of a large number of vibrations of the same pitch and of arbitrary phase. Phil Mag Series 5 1880;10(60):73–78.

Tunis AS. Monitoring structural changes in cells and tissues with high frequency ultrasound signal statistics. M.S. thesis. University of Toronto, 2005.

Tunis AS, Spurrell D, McAlduff D, et al. High frequency ultrasound signal statistics from mouse mammary tissue during involution. Proc IEEE Ultrason Ferroelec Freq Control Sympos 2004;768–771.